

# Application of pencil lead break (PLB) point source in the detection of interfacial defects in adhesive bonds.

PRATHURU, A., FAISAL, N., STEEL, J. and JIHAN, S.

2022

*The version of record of this article, first published in Journal of nondestructive evaluation, is available online at Publisher's website: <https://doi.org/10.1007/s10921-022-00898-7>*



# Application of Pencil Lead Break (PLB) Point Source in the Detection of Interfacial Defects in Adhesive Bonds

Anil Prathuru<sup>1</sup> · Nadimul Faisal<sup>1</sup> · John Steel<sup>1</sup> · Sha Jihan<sup>1</sup>

Received: 16 March 2022 / Accepted: 2 September 2022  
© The Author(s) 2022

## Abstract

The presence of kissing bonds (zero-thickness disbond) along the interface of an adhesive bond is highly detrimental to its strength and longevity. The detection of these kind of defects has previously been attempted using several techniques such as ultrasonic, infrared thermography, and X-ray spectroscopy, etc. This study aims to assess the effectiveness of pencil lead break (PLB) tests as a source in detecting the defects distributed along the interface of an adhesive bond. The defects were introduced artificially using polytetrafluoroethylene (PTFE) spray along one of the interfaces of the adhesive bond fabricated with aluminium plates bonded with an epoxy adhesive. Three different interfacial defect area percentages, 0%, 25% and 40% and three adhesive layer thicknesses (i.e., 0.1 mm, 0.25 mm, and 0.5 mm) were considered. The PLB tests were conducted, and the recorded signals were analysed to assess the variation of AE features with the defect area percentage and adhesive layer thicknesses. Different source-sensor location configurations were also considered. The 200 kHz-highpass component of the recorded signals was found to be sensitive to the presence of the interfacial defects. The duration above a chosen threshold was found to be the distinguishing factor between the different defective specimens. Of the different sensor-source configurations tried, the configurations with the PLB on the 0.5 mm side were seen to be sensitive to the presence of defects.

**Keywords** Metal-to-metal adhesive bonds · Acoustic emission · Pencil lead break test · Kissing bonds · Interfacial defects · Defect detection

## 1 Introduction

Adhesive bonds are applicable in various areas of material joining as a replacement to conventional joining processes and are desirable because of the ease of manufacture, nature of load and stress distribution and production costs. Due to various manufacturing and operational environment related factors, adhesive bonds are prone to several defect types, zero volume disbonds (kissing bonds) being one of the critical ones. Detection of kissing bonds is difficult due to their inherently small dimensions, particularly, their close to zero thickness. Regardless, several techniques based on ultrasonics [1], guided Lamb waves [2], non-linear dynamics [3] have been devised to both locate and size interfacial disbonds. Pencil lead break (PLB) test has conventionally been used as a simulated acoustic emission (AE) point source to understand

wave propagation in different materials and associated signal dampening and attenuation. PLBs have been used in the detection of weld defects [4] and to understand wave propagation in thin solids and wave guides. The validity of using PLB as an AE source has been studied using finite element (FE) models [5].

In this paper, the surface displacement and loading rates induced by a PLB have been calculated. Mathematical description of the PLB event has been provided based on the experimental and simulation data. The pencil lead free length and orientation angle with respect to the surface were shown to be critical to the loading. In another study [6], out-of-plane PLBs were shown to induce fundamental zero-order antisymmetric mode or flexural mode (A0) and zero-order symmetrical mode or extensional mode (S0) propagation in aluminium plates of thickness 5 mm. Simulations of in-plane and out-of-plane monopole and dipole AE sources in aluminium plates were carried out in another study [7]. The typical PLB test used in practice was shown to be equivalent to an out-of-plane monopole that induces a high amplitude A0 component and a very low amplitude S0 component. The

✉ Anil Prathuru  
a.prathuru@rgu.ac.uk

<sup>1</sup> School of Engineering, Robert Gordon University, Garthdee Road, Aberdeen AB10 7GJ, UK

suitability of these fundamental modes in the detection of adhesive bond defects, specifically kissing bonds has been studied in detail. Rokhlin et al. [8] studied the use of S0 mode transmission in single lap joint edge condition detection. More recently the use of A0 and S0 modes in mapping disbond between a stiffener and an aluminium plate was studied [9]. The use of correlation coefficients between the reflected signals at three excitation frequencies from a pristine and defective bond layer has been proposed as a measure of the degree of disbond. They implemented a windowed root mean square (RMS) method on the acquired signals to map the size and shape of the defect.

In another study, the use of the refracted, mode converted A0 wave in detecting the presence of a defect, based on numerical and experimental studies on a controlled disbond in a lap joint was proposed [10]. They observed mode conversion of the incident S0 into A0 across the bond line. Furthermore, based on the observed interactions of the S0 mode with the defect, they proposed specific locations within the specimen geometry to monitor defect scattered mode converted A0. This was shown to travel in a different direction to the incident wave making it unique to the defect. The difference between the defective and pristine bonds was shown to be the highest at 300 kHz. The use of low frequency (10–50 kHz) A0 in detecting developing cracks in composite repair specimens has been proposed by Diamanti et al. [11]. Reflection of the A0 mode from the crack edge and its time of flight with respect to the incident wave was measured and quantified against known crack lengths. The mode propagation was shown to be faster in the pristine bond compared to the base adherend. Using these relations, crack lengths and locations were predicted to a high accuracy. However, it must be noted that the specimens used were of a simple plate type and so the measurement of the time-of-flight (TOF) was straight forward. In the case of complex geometries, the proposed analysis will need to be modified to include the reflections and possible mode conversions. Mustapha et al. [12] used low frequency A0 based inspection method to locate and size a composite sandwich delamination defect. The magnitude and TOF of the reflected wave were related to the defect location and size. In addition, the correlation of the reflected signal from a defect and a pristine specimen has been calculated using the Hilbert-Huang transform. However, due to competing mechanisms of wave damping and mode velocity changes induced by the presence of the delamination, a unique relation between the delamination size, location and the calculated parameters could not be obtained. In addition, mode propagation characteristics of the sandwich specimens were not considered in this study.

Rucka et al. [13] used scanning laser doppler velocimetry (SLDV) in the detection of induced voids and kissing defects in adhesively bonded lap joints. A 200 kHz sine wave was used to A0 propagation in the lap joint. A weighted root mean

square (WRMS) estimation was carried out on the gathered surface velocity data at several locations resulting in a defect map. The time window and the individual weights in the WRMS were optimised to increase the contrast in the maps. The calculated WRMS value was found to be higher directly above the location of the introduced defects which relates to the amplitude of the propagating wave within the defect area.

Mori et al. [14] studied the transmission of the A0 mode through adhesive bonds with different adherend surface preparation methods. The variation of the transmission coefficients with the surface condition and consequently the tangential stiffness of the interface have been quantified by defining the peaks and notches in the frequency response of the transmitted wave. The induced A0 mode with a central frequency of 200 kHz was shown to be sensitive to the interfacial condition.

It is evident that the A0 and S0 fundamental Lamb modes are capable of detecting defects in adhesive bonds and also that PLBs generate these wave modes in plate structures. However, this apparent connection has not been made yet in understanding the application of PLB in adhesive bond defect detection. In scientific studies, the detection of the defects relied on the generation and propagation of a specific frequency propagating along the adhesive bond line. The same frequencies could also be generated by a simple PLB test thus negating the need for complex signal generation and acquisition methods. However, given the manual nature of the PLB test and the possibility of inducing multiple modes within the plate structure, there is a need to understand the suitability of PLB for adhesive bond defect detection. The current study attempts to address this gap.

The current research, for the first time, establishes the standard PLB test as a viable method to identify defective interfaces in adhesive bonds. The use of pencil lead break (PLB) as a signal point source along with an AE sensor adhesive bonds defect detection is investigated. Artificial defects were introduced along the adhesive-metal interface to simulate kissing bonds. Two interfacial defect area percentages (25%, 40%) were considered, and the acquired signals were compared to those from a pristine specimen. Though these values were chosen arbitrarily, they were used to establish the sensitivity of the proposed method. As will be shown later, the method was able to detect a large 10 mm × 10 mm (representing 1.67% interfacial defect area) defect with ease. The intention was to test the efficacy of the method in detecting distributed smaller defects. Frequency content of the acquired signals was analysed and parameters to differentiate the different defect percentages are proposed. In contrast to the complex guided wave methods used in the detection of the kissing bonds, the proposed method is simple and can easily be replicated for a given specimen. The use of normalisation and adoption of energy ratios in the signal processing

method meant that the results are less affected by the sensor mounting and test repeatability.

## 2 Materials and Methods

The sample preparation, PLB test set-up and signal processing methods have been discussed elsewhere [15] and are referred here briefly.

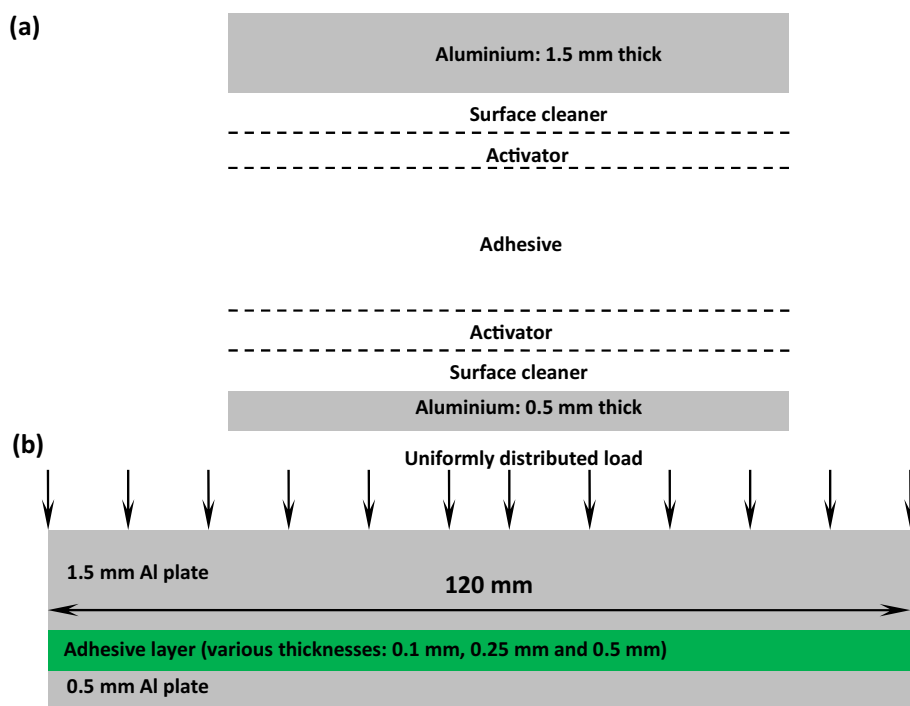
### 2.1 Specimen Details

The adhesive joints were made by joining two aluminium plates with dimensions 120 mm × 50 mm × 1.5 mm and 120 mm × 50 mm × 0.5 mm. This section explains the methodology of specimen preparation and specimen quality control. The interface bonding conditions were varied. For defect detection tests, pristine specimens with no defects along with specimens with 25% and 40% defect area distributions along one of the interfaces have been prepared.

The as received aluminium plates were cleaned with Loctite®7063™. This was done on both the faces of the adhesive joint. Next, the plate surfaces were sprayed with Loctite®7649™ activator. Temper half hard (AL000730, size: length 120 mm, width 50 mm and thickness 1.5 mm, and AL000645, size: length 120 mm, width 50 mm and thickness 0.5 mm; Good Fellow Ltd., Cambridge, UK) aluminium plates were selected for this study.

All the specimens were prepared using a Loctite® 9430 epoxy adhesive. Fig. 1 describes the scheme of the adhesive bond specimen preparation. adhesive layer thicknesses chosen were 0.1 mm, 0.2 mm and 0.5 mm based on the standard thicknesses used in adhesive bonds. After the initial degreasing of the metal plate surfaces, Loctite®7649™ surface activator was sprayed on. After this, bond defects were introduced along the interface between the 0.5 mm thick plate and the adhesive layer. The interfacial defects were introduced by applying a thin PTFE coating sprayed through prefabricated templates on to the 0.5 mm thick aluminium plate. The use of the template ensures that there is no overspray on the plate surface and hence prevents overlap between neighbouring defects. This introduced an array of circular defects on the surface of the aluminium plate. The number of passes of the PTFE spray over the plate was kept constant across all the specimens. The thickness of the circular defects was not more than 10 μm as measured with a micrometer. The template used to create the interfacial defects has a uniform distribution of holes. The templates used and the aluminium plate with the defects are shown in Fig. 2. After the PTFE spray has dried on the plate, adhesive was applied. Bond gap was controlled using aluminium shims, introduced to maintain a gap equal to the desired adhesive layer thickness. After the application of the adhesive, a uniformly distributed load (20 N) was applied, and specimens were cured for 2 days at about 25 °C and a relative humidity of about 30%. In total, 9 different specimen types were manufactured.

**Fig. 1** Schematic of specimen preparation methodology: **a** scheme of application of surface cleaner, activator and adhesives, and **b** application of uniformly distributed load



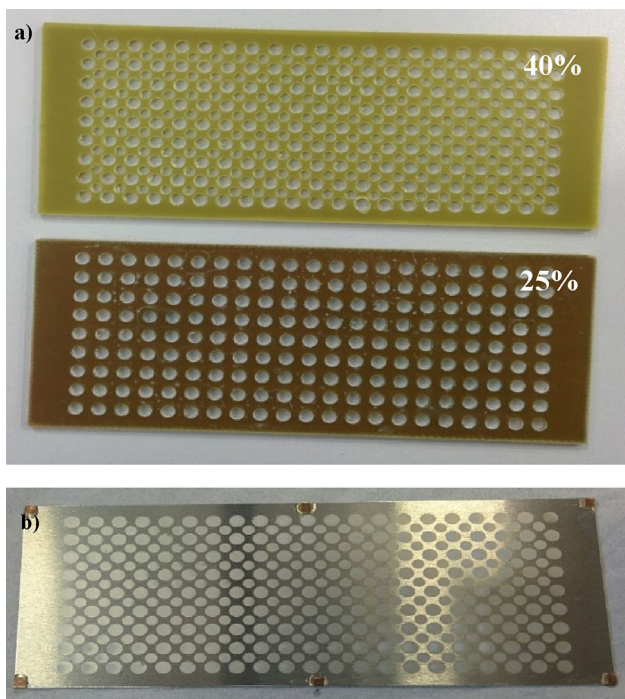


**Fig. 2** a Templates used for the defective specimen preparation for experiments, and, b PTFE sprayed surface with 40% defect area percentage

### 2.2 Pencil Lead Break (PLB) Test

The AE sensors from Physical Acoustics Corporation, Micro-80D, with a frequency response range of 100 kHz to 900 kHz and a resonant frequency of 325 kHz were used. The

sensor exhibits a close to flat response across the frequency range, except at the resonant frequency where the response peaks. Pre-amplifiers of type PAC series 1220A were used in combination with the sensors. An in-house developed signal conditioning unit (SCU) was used in addition for further amplification or de-amplification as required. Co-axial BNC cables were used to connect the sensors and the amplifiers to a BNC block (National Instrument, NI-2110) which was connected to a NI-6115 PCI-express data acquisition card. The block diagram of the setup used is shown in Fig. 3. Each specimen was placed on a wooden block with a V-shaped groove in the middle so that it is simply supported over a length of 2 cm on each side.

The AE sensor was mounted on the specimens using aluminium tape. The thickness of the aluminium tape was less than 15 μm and hence it is not likely to significantly affect the wave propagation characteristics of the aluminium plates. Silicone sealing grease was used as the couplant between the sensor and specimen with the sensor being held down by aluminium tape against the specimens. The sensor mounting procedure was tested for signal acquisition repeatability by removing the aluminium tape and the sensor and remounting. PLB tests were conducted at the same location to test the repeatability and ensure that the uncertainty associated with the sensor mounting procedure can be eliminated in signal analysis (Fig. 4). Two different sensor-source location configurations were considered. The first has the sensor and the source (i.e., PLB) on the opposite faces of the adhesive bonded specimen. The sensor was located at the geometrical centre of the face in this configuration. This configuration

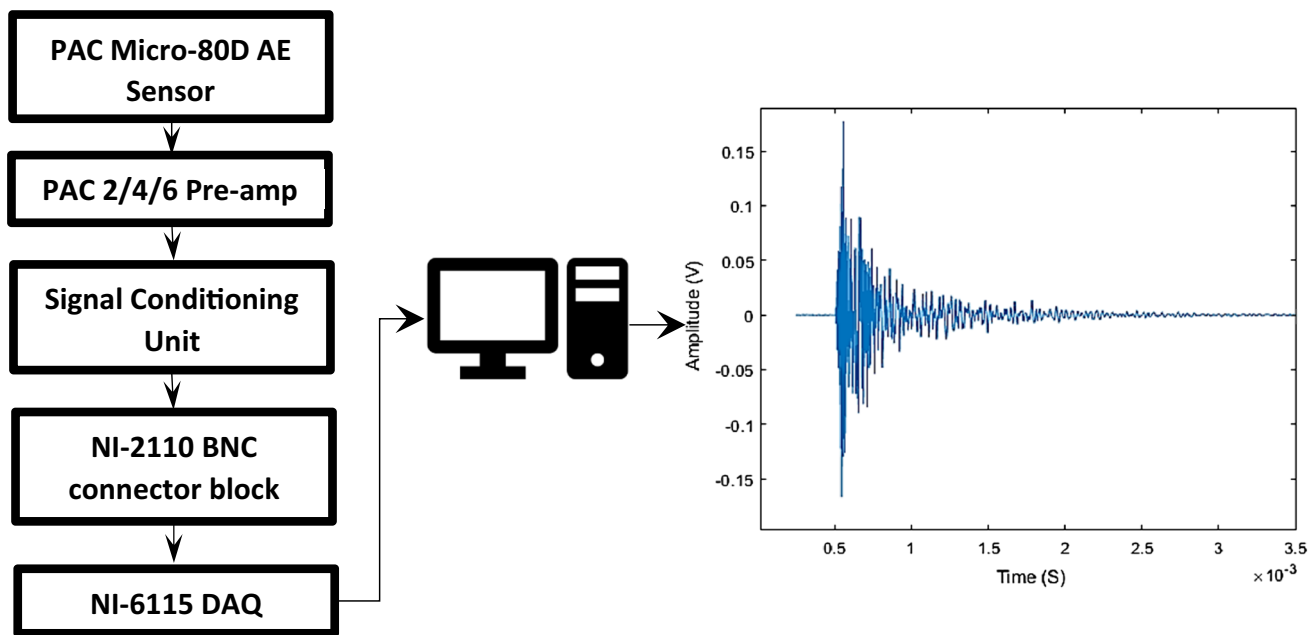


**Fig. 3** Schematic of AE signal acquisition

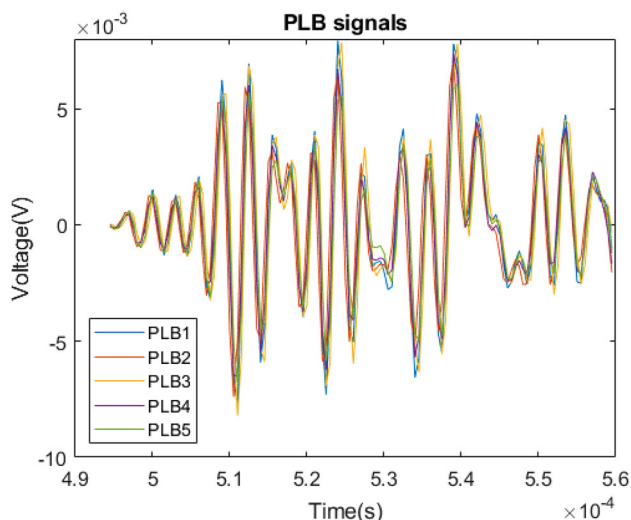


**Fig. 4** Repeatability of the PLB tests on 0.5-0.1-1.5 at a distance of 40 mm from the sensor

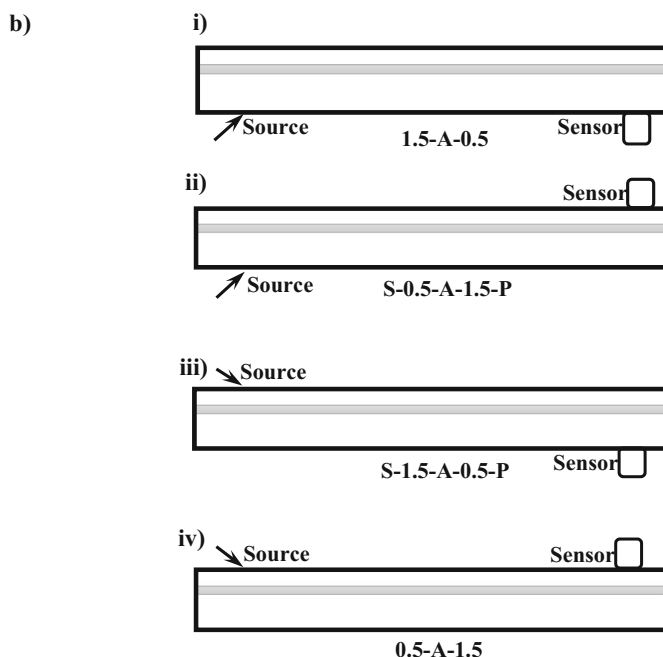
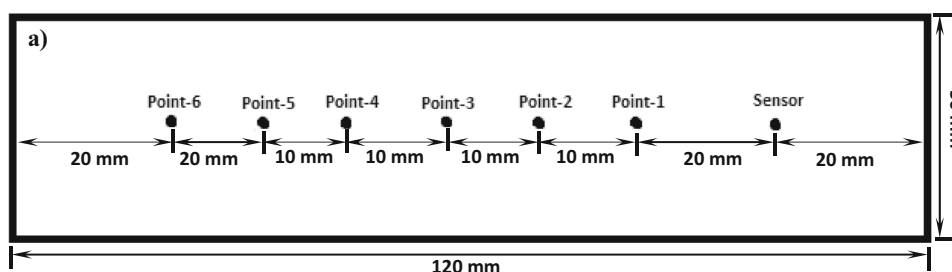
was chosen to study the wave transmission and attenuation through the thickness of the adhesive layer. The second configuration has both the source and sensor on the same face of

the adhesive bonded specimen. Seven different points were marked on both the faces of each specimen and the PLB tests were carried out at these points. The location of these points is shown in Fig. 5a. A commercial mechanical propelling pencil with an in-house machined guide-ring was used to generate simulated AE sources by breaking a 0.5 mm diameter and 2–3 mm length 2H pencil lead, as recommended by ASTM standards (E976-99) [16]. Various specimen-sensor configurations are shown in Fig. 5b. To ensure repeatability, five PLBs were recorded at each of the positions as per Fig. 4.

### 2.3 Specimen Name Convention

With the given specimen geometry of two aluminium plates bonded with an adhesive layer, 4 different sensor-PLB source configurations have been assessed for their ability in detecting the interfacial defects. The first configuration type had both the sensor and PLB source on the same metal plate. This gave 2 configurations with the 0.5 mm and 1.5 mm plates of the adhesive bond (Fig. 5b(i), b(iv)). The second type had the sensor and source on the opposite faces of the specimen. For

**Fig. 5 a** Sensor and PLB source locations on the specimens (not to scale, schematic). **b** PLB test configurations showing source & sensor locations



these configurations, the letters 'S' and 'P' have been used to indicate sensor and the PLB source. For example, S-0.5-0.1-1.5-P (Fig. 5b(ii)) indicates that the sensor was located on the 0.5 mm plate, PLB source on the 1.5 mm plate and the adhesive layer thickness was 0.1 mm. The interfacial defect area percentage, if any, is added to the specimen's name. Where the specimen's name does not have 'S' and 'P', test configuration is of the first type and the sensor, PLB source were located on the plate of thickness equal to the left most value in the specimen's name. For example, 0.5-0.1-1.5-40% indicates that the adhesive layer thickness is 0.1 mm and that the sensor and PLB source were on the 0.5 mm plate and the interfacial defect area percentage was 40%. The configurations and corresponding naming conventions are shown in Fig. 5b.

## 2.4 AE Signal Processing

AE signals were acquired at a rate of 2 MS/s in all the recordings conducted. The sampling frequency was chosen to be more than twice the maximum frequency being investigated. Five repetitions were conducted at each point on the specimen and the acquired signals after each test were stored as binary (.bin) files. Signal processing was done using the codes written in data analysis software (MATLAB). The energy content of the signal was measured by calculating the total area of the absolute magnitude-time profile.

$$E = \int |V| dt, \quad (1)$$

where E is the signal energy, V is the signal voltage as a discrete function of time and t is the time. The rise time, decay (fall) time and hit rate were calculated for each signal record by using a threshold value above the noise level. Different values of the threshold were considered to maximise the defect detection capability of the data processing technique. In cases where the threshold was based on the peak amplitude, it was taken to be 2% of the peak. Digital filters (Chebyshev type II) were applied to the recorded signals to estimate and quantify the changes induced in the signals by the interfacial defects in the specimens. In this technique the signal was divided into windows of 300 samples each and the local maxima was calculated in each window. These values were then combined to create a re-sampled signal. Signal-to-noise ratio (SNR) was calculated, using Eq. 2 below, in each window using the local maximum of the signal. The noise floor for this calculation was taken to be the noise recorded from the AE sensor without any AE activity

$$\text{SNR} = 20 \log_{10} \left( \frac{V_2}{V_1} \right) \quad (2)$$

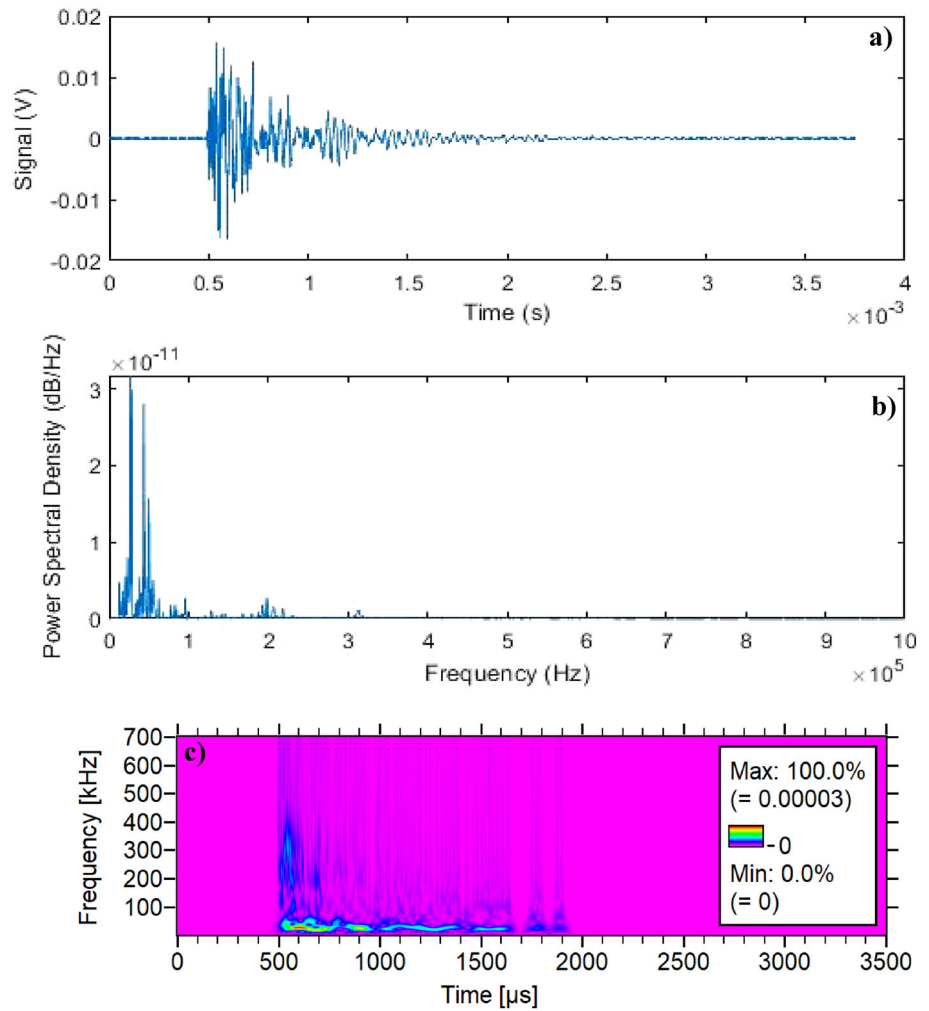
where SNR is the signal-to-noise ratio,  $V_2$  and  $V_1$  are the signal voltage and the noise floor recorded from the AE sensor respectively. The calculated SNR values were then normalised to a scale of 0 to 1. Calculation of the SNR and subsequent normalisation enabled the comparison of different signal records on a common platform and to understand signal decay rates.

## 3 Results and discussion

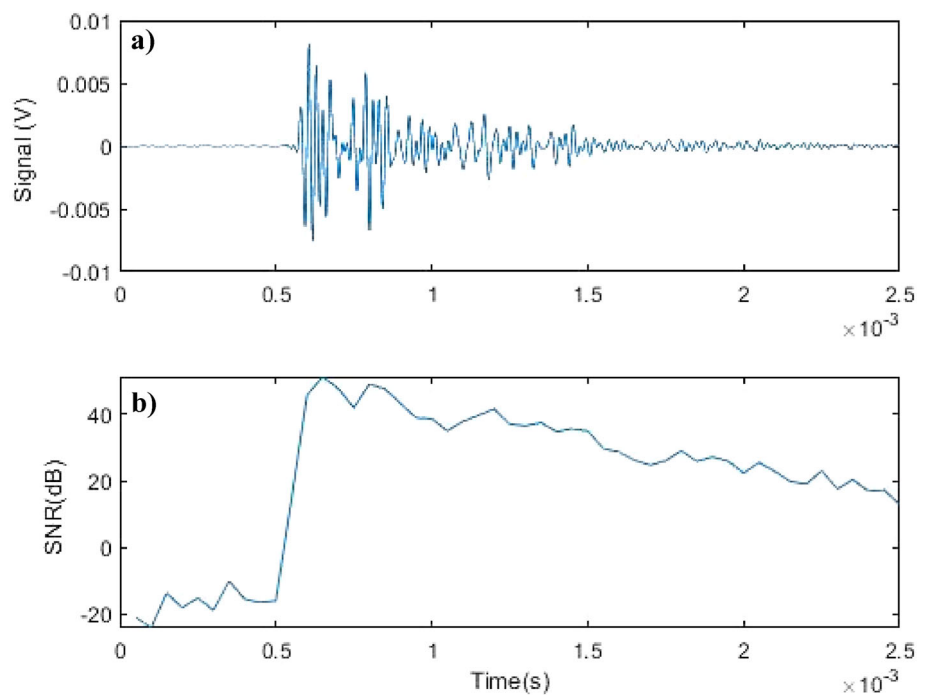
### 3.1 Signal Transmission in Metal Plates

The signal transmission in the aluminium plates is first studied. To this end, a one-off experiment was conducted with the 1.5 mm plate with 2 sensors mounted on the surface at 40 mm and 80 mm from the PLB source location. This gave a path difference of 40 mm between the two sensor locations. Based on this, the velocity of the first arriving wave was estimated. This, in conjunction with the wavelet transform, was used to understand the wave propagation in the plates. Based on the calculated wave velocities, it is concluded that the PLB signal has a low frequency low amplitude S0 component reaching the sensor first followed by a high frequency high amplitude A0 component. The peak amplitude of the signal lies within the high frequency range. Figure 6 shows the PLB signal recorded on the 1.5 mm plate. Several reflections are seen (Fig. 6c) within the sample given the small dimensions and there was significant overlap as expected due to the proximity of the boundaries to the source location. The significant amount of low frequency energy within the signal is to be noted given the lower sensitivity of the sensor used at frequencies below 100 kHz. To isolate the low frequency component of the recorded wave signal on the 1.5 mm plate, a 50 kHz lowpass filter was employed and the signal to noise ratio of the filtered signal was calculated. The plot of the filtered component and the corresponding SNR vs time is shown in Fig. 7. The high SNR despite the low sensor response in this frequency range is to be noted. The same was observed with the 0.5 mm plate. A low frequency, low amplitude S0 reached the sensor first followed by a high frequency, high amplitude A0 component. The rest of the signal constituted the reflections from the plate boundaries. This signal too exhibited significant activity in the low frequencies. In both the 0.5 mm and 1.5 mm thick plates, the out-of-plane displacement decreases considerably as the frequency increases. For example, in the 0.5 mm thick plate, the out-of-plane displacement at 30 kHz is ~ 390 nm, whereas that at 300 kHz is ~ 13 nm and the estimated surface velocities, used as an indicator of the sensor response, are calculated to be ~ 0.08 m/s and ~ 0.0025 m/s at 30 kHz and 300 kHz respectively. Surface velocity was calculated based on the frequency and the surface displacement. Frequency was used to calculate the

**Fig. 6** **a** PLB signal acquired from the 1.5 mm aluminium plate along with the **b** power spectral density and **c** wavelet transform



**Fig. 7** **a** 50 kHz-lowpass component of a sample PLB signal on 1.5 mm plate and **b** corresponding SNR



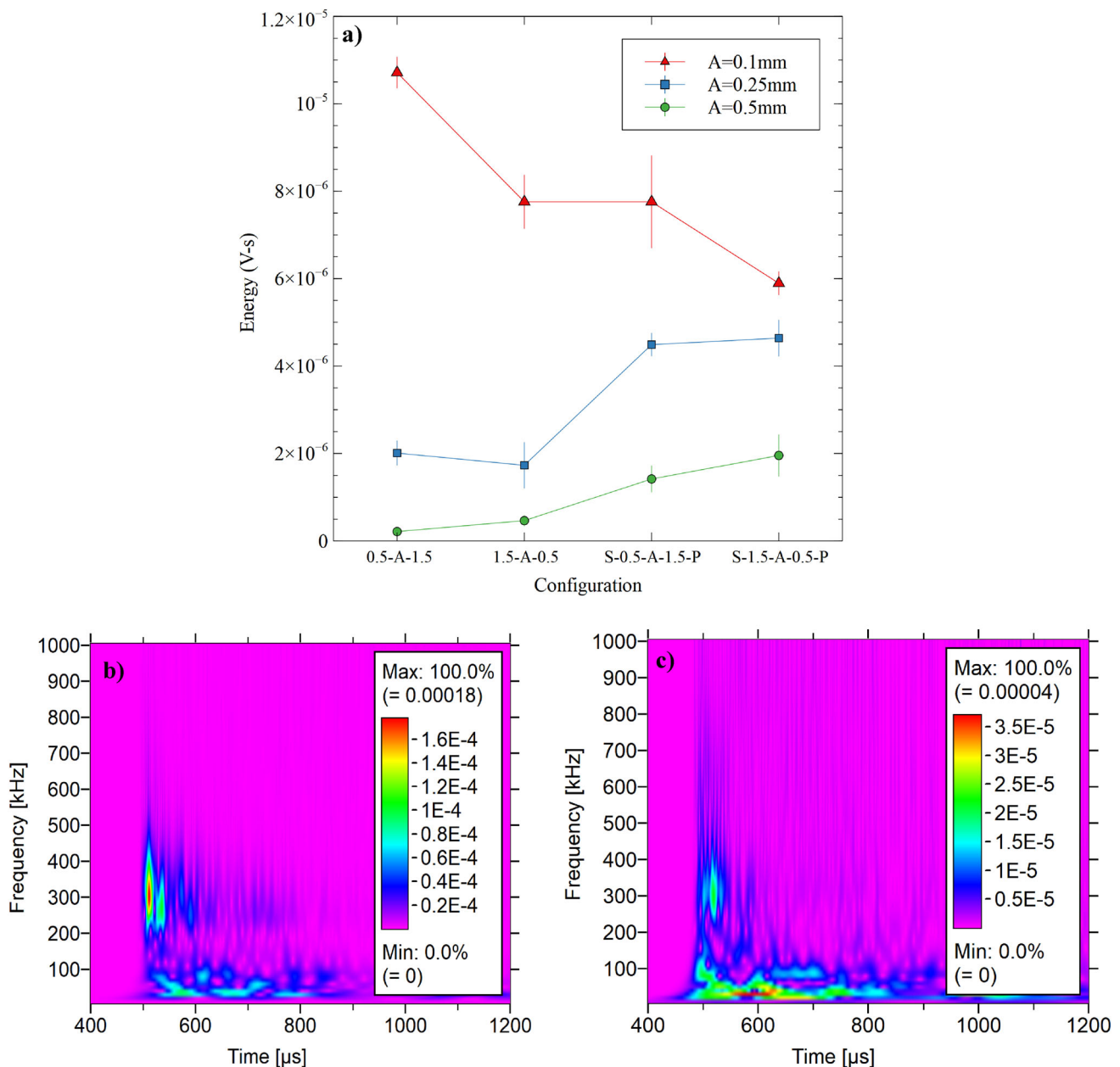


**Fig. 8** a Energy content of signals with different configurations and adhesive layer thicknesses, b Sample WT plot of 0.5-0.1-1.5, c sample WT plot from S-1.5-0.1-0.5-P

time period. Assuming sinusoidal surface motion, the surface displacement and the time period were used to calculate the average surface velocity for the wave transmission. Out-of-plane displacement with the 1.5 mm plate at 30 kHz is  $\sim 93$  nm and at 300 kHz is  $\sim 6$  nm and the corresponding surface out-of-plane velocities are  $\sim 0.0175$  m/s and  $\sim 0.00125$  m/s respectively. The use of the specimen surface velocity as representative of the sensor signal is proposed by Sause and Horn [17]. They compared the surface velocity of a steel plate obtained on a steel plate with a cosine

bell function as the simulated PLB source with experimental sensor data from PLB tests. A very good correlation was shown between the simulated and experimental data. The large difference between the surface velocities at 30 kHz and 300 kHz for both the 0.5 mm and 1.5 mm plates explains the high amount of low frequency content seen in the signals. It is also to be noted that though the sensor used has a frequency band of 100 kHz–900 kHz, it is still sensitive to lower frequencies though not to the same level. Similar behaviour is expected with the adhesively bonded specimens, the effect of

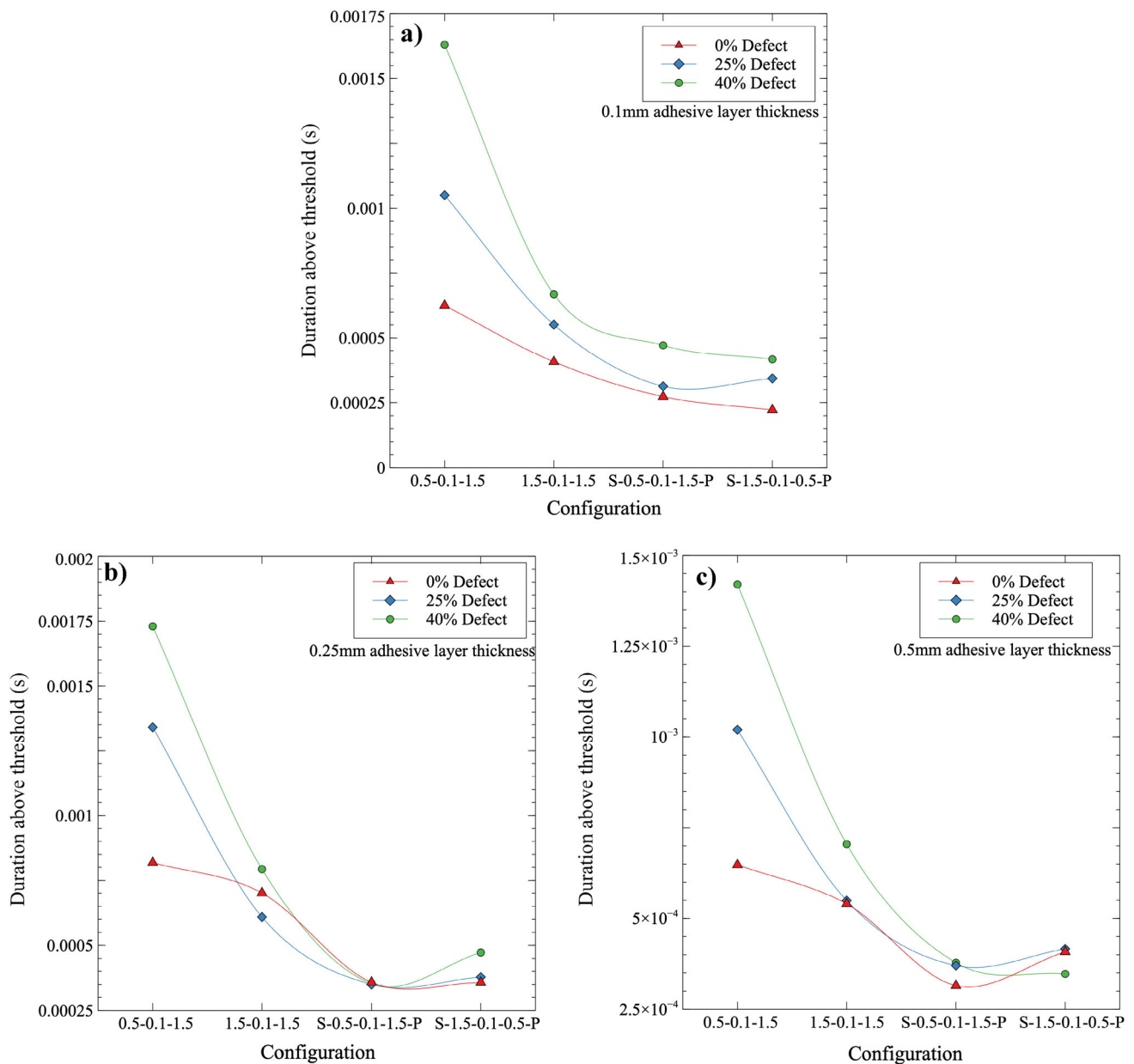


**Fig. 9** Variation of time above threshold of the 200 kHz high pass component with specimen configuration and defect area percentage for **a** 0.1 mm, **b** 0.25 mm, **c** 0.5 mm thick adhesive layer

the adhesive damping on the signal frequency content being of interest.

### 3.2 Sensor-Source Configuration

The difference between the different sensor-PLB configurations is discussed here. It was previously shown that the wave propagation in a multi-layered adhesive bond can be sufficiently approximated by the dispersion curves of the constituent metal plates [18, 19]. Instead of acting as a single structure, the constituent plates act as individual laminates

each with their own wave propagation characteristics. In this case, the dispersion curves of the metal plate on which the sensor was mounted were mapped onto the wavelet transforms of the PLB records. With each adhesive layer thickness, the variation of the signal energy content with respect to the sensor-source configuration is shown in Fig. 8a. As seen, with all the general trend is a decrease in the signal energy switching from a configuration with the sensor and the source on the same side to a configuration with these on the opposite side. Comparing signal WTs from the configurations with PLB and sensor on the same side and those with these two

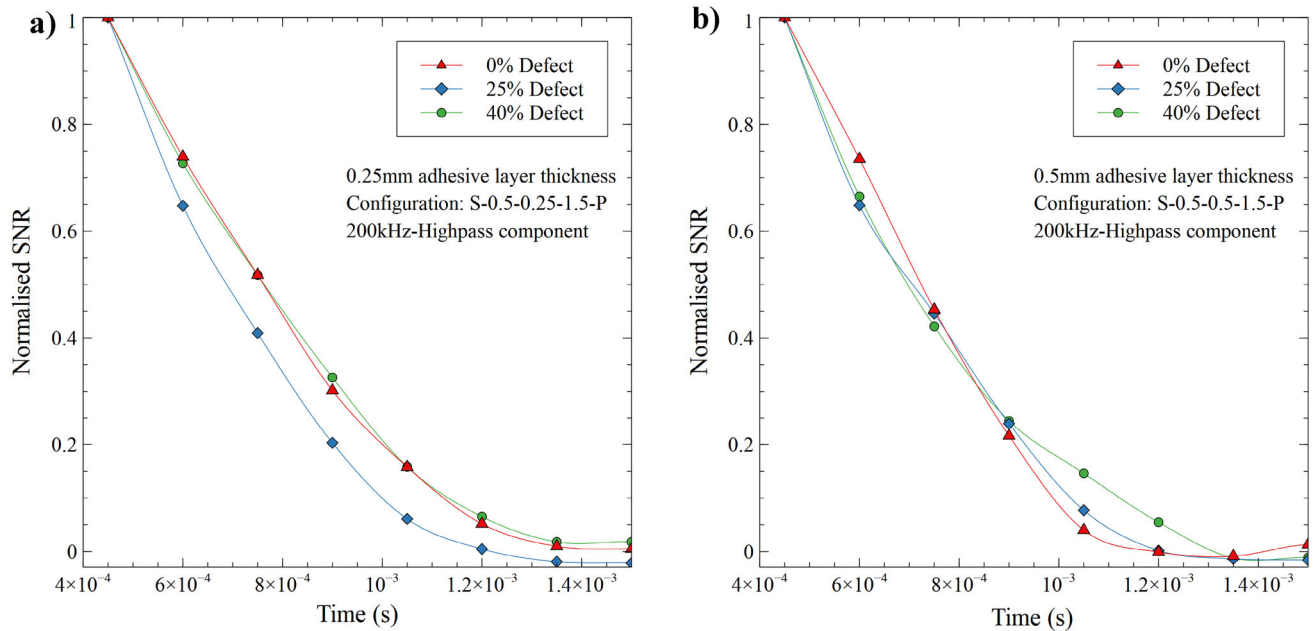


**Fig. 10** Normalised SNR vs time of the 200 kHz-Highpass components from various defective specimens with the configuration S-0.5-A-1.5-P and adhesive layer thickness of **a** 0.25 mm, **b** 0.5 mm

on the opposite faces, the signal decay is more rapid in the latter case. An example is shown in Fig. 8b, c. This translates to a smaller duration above threshold with the latter case. Having the sensor and source on opposite faces of the specimen decreased the energy content of the signal. This implies damping through the adhesive layer, despite similar energy ratios. Regardless of the decay rate, all configurations were analysed for defect detection, and it was found that not all configurations were sensitive to the presence of the defects.

The effect of the configuration on the acquired signals with different thicknesses can be seen from Fig. 9. The time above threshold of the signals acquired on the adhesive bonded specimens with various adhesive layer thicknesses and defect area percentages is shown in this figure. As seen, with the various configurations, with the 0.1 mm thick adhesive layer specimen, there is a clear distinction between the pristine and defective specimens. The configuration 0.5-A-1.5 is seen to be the most sensitive with the other configurations showing smaller, though distinguishable difference in the time above threshold. Also, a decrease in the time is the general trend seen with the various specimen types with changing configuration. The principal difference between the configurations is the signal travel path and the proximity of the signal source to the interface with the defects. With the configurations where the sensor and source are located on the opposite faces of the specimen, the signal has to travel through the adhesive to reach the sensor. Literature suggests that the effect of signal transmission through an adhesive layer is the reduction of the high frequency content of the signal [18].

With the 0.1 mm adhesive layer specimen, all the configurations appear to be capable of differentiating between the different defective specimens, though some configurations to a smaller extent than the others. With higher thicknesses, the signal attenuation was high enough that the recorded signal was not capable of distinguishing between the different defective specimens. This is seen in Fig. 10 where the normalised SNR of the signal's 200 kHz-highpass component is compared between the defective specimens in the configuration S-0.5-A-1.5-P. As seen, the curves are close to coincident, making defect detection in these specimens harder than it is with the 0.1 mm thick adhesive layer specimen.

### 3.3 Effect of Adhesive Layer Thickness

The effect of the increasing adhesive layer thickness is presented in this section. The overall energy content of the signal is first calculated and compared between the three adhesive layer thicknesses (i.e., 0.1 mm, 0.25 mm, 0.5 mm) studied. The change of the amplitude decay rate of the three thicknesses is shown in Fig. 11a. As seen, the higher thicknesses exhibit faster signal decay over time. The rate of decay can be seen more clearly in the time vs frequency domain. Figure 12 shows sample WT plots from the specimens of the three thicknesses.

The averaged signal of each sample is subjected to three digital filters (i.e., 50 kHz lowpass, 50–200 kHz bandpass, and 200 kHz highpass). The calculated energy ratio of these

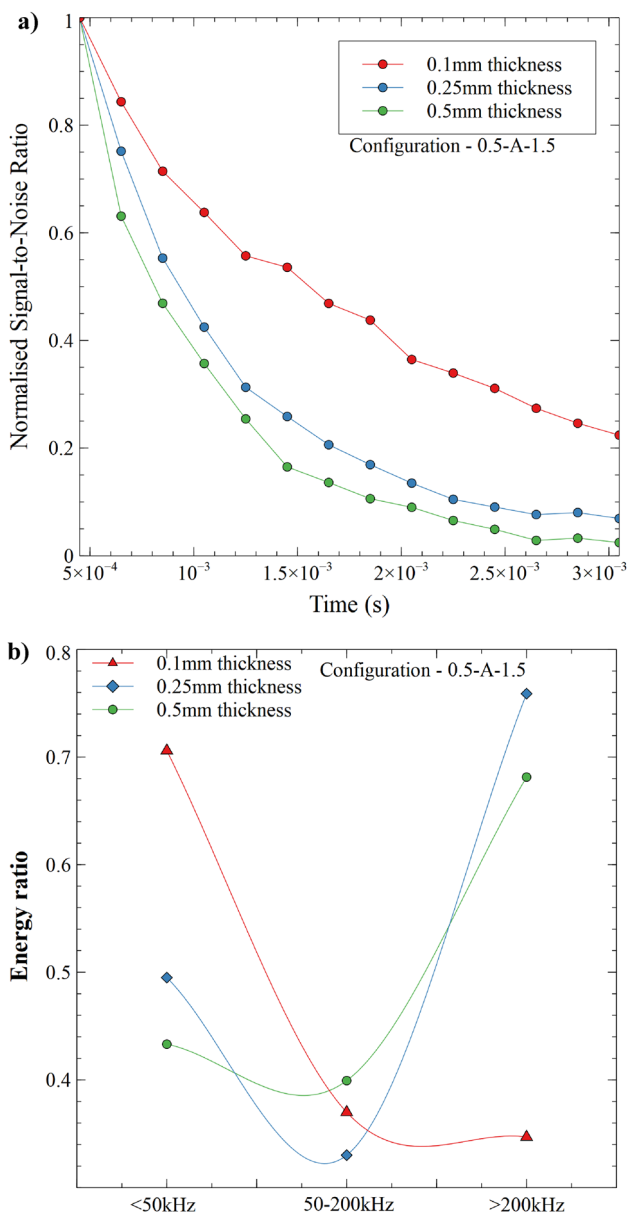


Fig. 11 a Signal SNR and b Energy ratio variation with adhesive layer thickness

filtered signal components for the 3 adhesive layer thicknesses is shown in Fig. 11b. The energy ratio is calculated as the ratio of the energy of the filtered component to the total energy content of the signal. A clear shift of energy from low to high frequencies is seen with increasing adhesive layer thickness. This is seen from the WT plots for the three thicknesses shown in Fig. 12. Increase in the thickness of the adhesive layer leads to the decrease in the degree of constraint applied by the much stiffer adherends. This leads to easing of the deformation of the adhesive layer. The magnitude of the surface displacement in the adhesively bonded multilayer structure is higher at lower frequencies compared

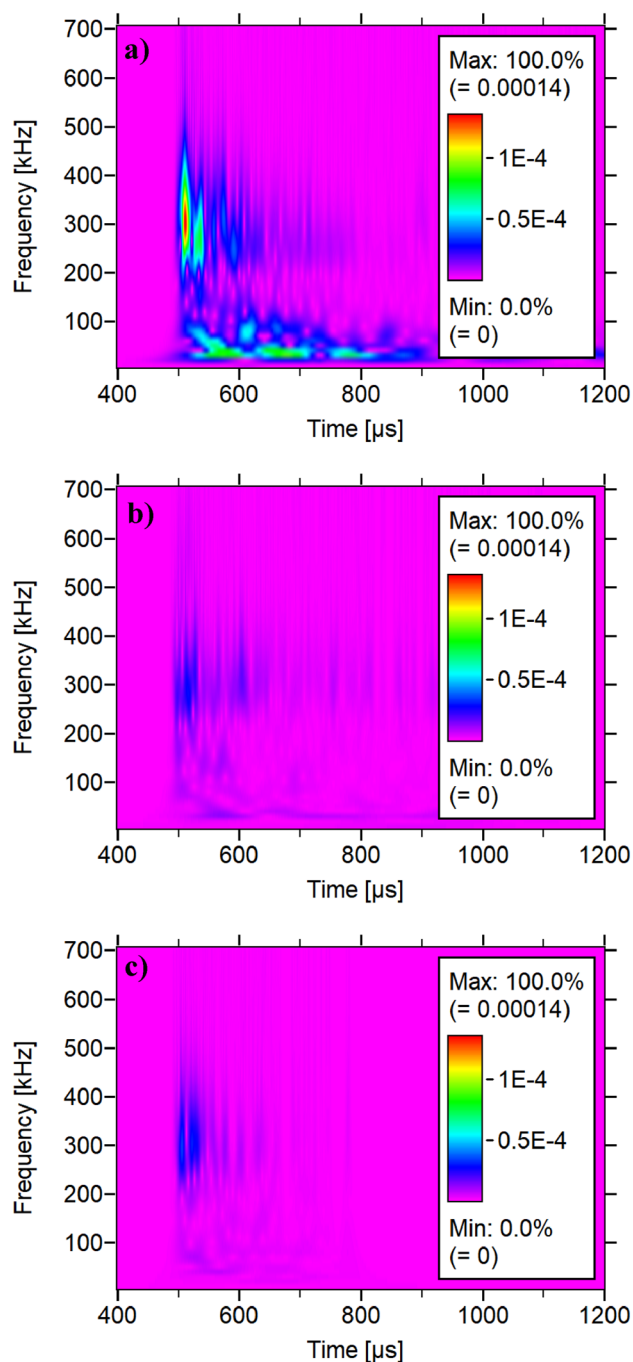


Fig. 12 Sample wavelet transform plots of PLBs on specimens with a 0.1 mm, b 0.25 mm and c 0.5 mm thick adhesive layers in the configuration 0.5-A-1.5

to higher frequencies. This also translates to a higher surface velocity at lower frequencies. Hence, these are expected to experience a higher degree of damping compared to high frequency waves whose associated surface deformation and corresponding surface velocity are significantly lower. This could be the most-likely reason behind the shift of the energy distribution to higher frequencies with increasing thickness.

At higher thicknesses, the signal exhibits resonance like behaviour with high amplitude at a frequency close to that of the resonant frequency of the sensor. At higher thicknesses, the wave propagation induced deformation of the adhesive layer is not constrained leading to higher damping of the propagating waves, especially at lower frequencies, as evidenced by the energy ratio plots for the different thicknesses (Fig. 11b).

### 3.4 Effect of the Presence of Defects

To test the effectiveness of the PLB method in identifying and predicting the presence of single large defect, the same sample preparation procedure with PTFE has been followed in preparing a specimen with an approximately square shaped defect along with some smaller circular defects. The interface surface before bonding is shown in Fig. 13a. The WT obtained from a PLB on this specimen is compared to that from a pristine specimen is shown in Fig. 13b and c. There is a clear difference between these two WTs showing that the

technique can detect interfacial defects. The observed difference is particularly in the  $> 200$  kHz frequency band. In this case, the high frequency A0 mode, propagating in the 0.5 mm thick plate, that arrives at the sensor after the S0 mode was seen to be sensitive to the presence of the defect.

The effect of the defects on the observed signal records will be discussed for each thickness in this section. With 0.1 mm of adhesive layer thickness, the signals were processed as mentioned previously with an averaged signal calculated in each case. The averaged signal was resampled with a frequency of 1666 Hz. The SNR was then calculated with the resampled signal and the values were normalised to a scale of 0–1. The comparison of the signal decay between the adhesive bonds with the defective interfaces and those with a pristine interface is shown in Fig. 14. The shown plots are of the 200 kHz-highpass filtered signal, with the configuration 0.5-A-1.5. As seen, the time taken for the normalised SNR to reach '0' is longer for the defective specimens. The signal behaviour can be clearly seen from the WTs from the different defective specimens.

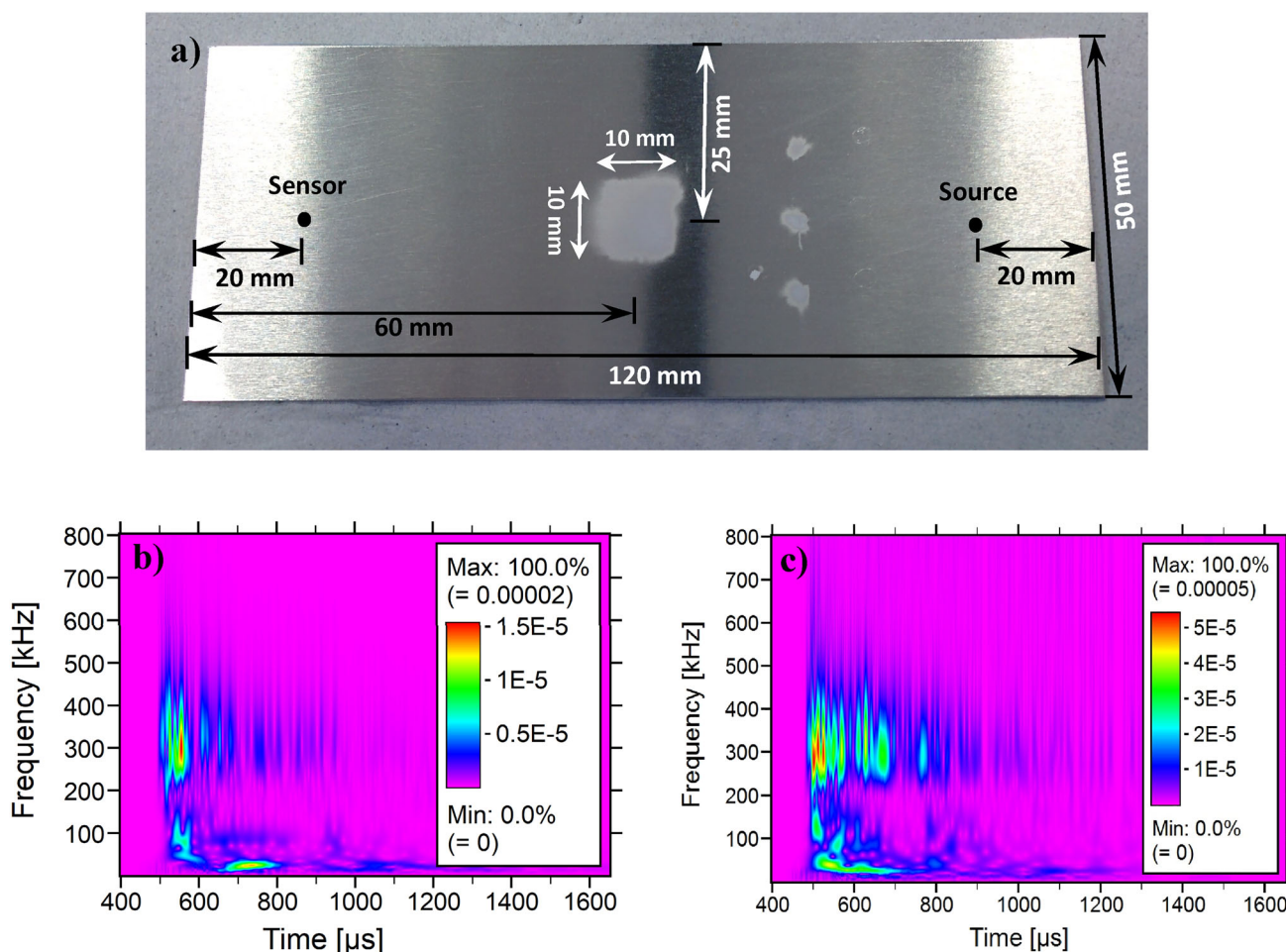


**Fig. 13** a Aluminium plate of size 120 mm × 50 mm × 1.5 mm with PTFE sprayed defect of size (10 mm × 10 mm) and location of AE sensor and PLB as sources, b WT of pristine specimen with no defect, and c WT of specimen with defect, in the configuration 1.5-A-0.5

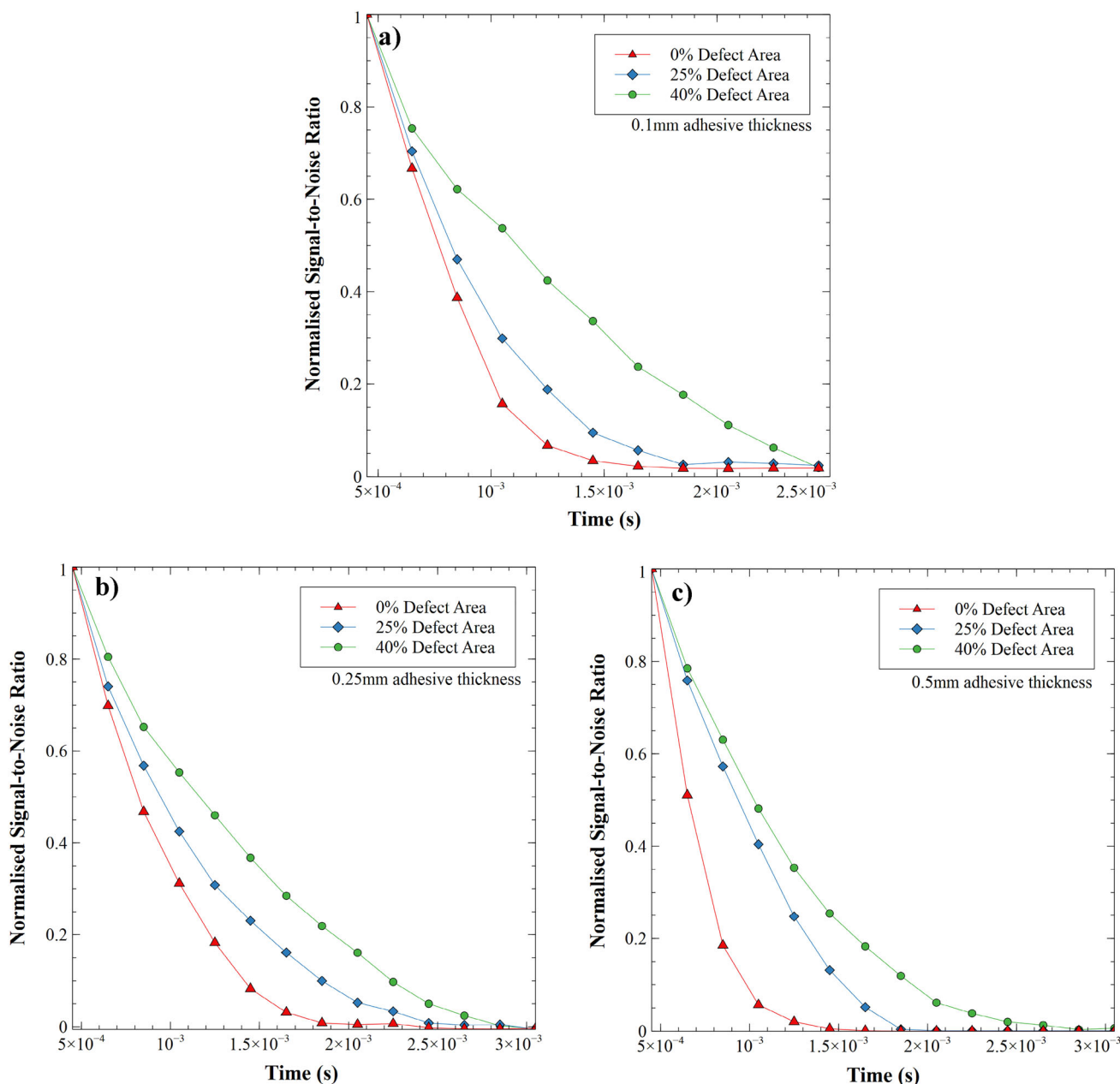


**Fig. 14** Decay of 200 kHz-highpass component expressed as SNR with respect to time with defective specimens of various thicknesses, **a** 0.1 mm thick, **b** 0.25 mm thick, **c** 0.5 mm thick adhesive layered bonds, in the configuration 0.5-A-1.5

In Fig. 15 are shown sample WTs of the 0.5 mm thick adhesive layer specimens with different defect area percentages, in which the increase in the low frequency activity can be clearly seen with the configuration 0.5-0.5-1.5. With the configuration S-1.5-0.5-0.5-P however, the opposite phenomenon was observed. It has to be noted here that, though in the both the configurations the pencil break was on the 0.5 mm plate, the sensor was mounted on the 0.5 mm plate in the former configuration, adjacent to which the defects are located, whereas it is on the 1.5 mm plate in the latter. Regardless, both the configurations show a clear distinction

between the different specimen defect area percentages. Such a distinction was not observed with the other configurations however, and so the results are not shown here. The energy associated with the high frequency component decreased with increasing defect area percentage with 0.25 mm and 0.5 mm adhesive layer thicknesses. This is represented by the energy ratio, calculated as the fraction of the total energy associated with each energy band.

The energy ratios for the 50 kHz-lowpass, 50–200 kHz bandpass and 200 kHz-highpass components are shown in Fig. 16 for all the three adhesive layer thicknesses. The energy

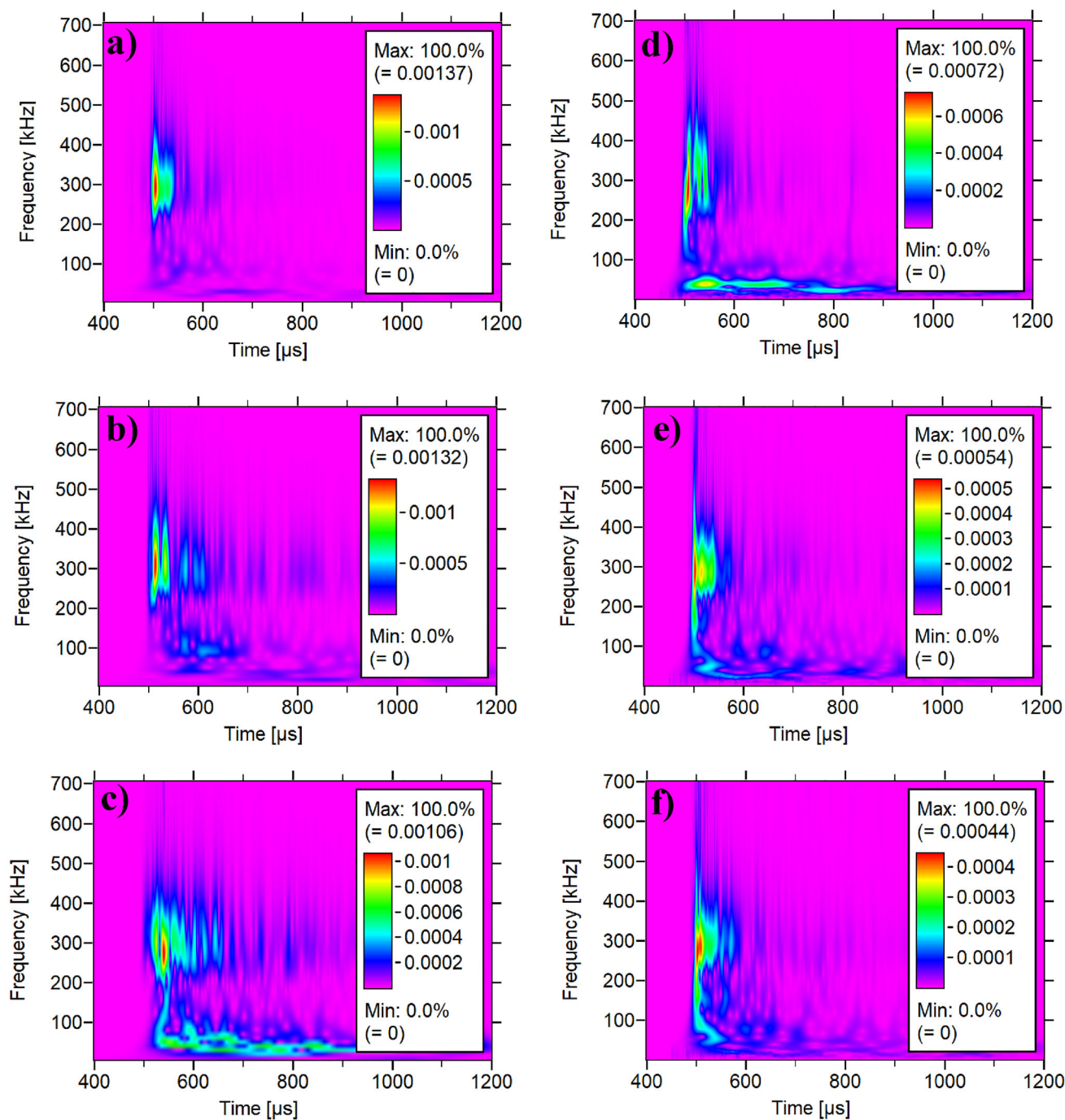


**Fig. 15** WTs of PLB tests at 80 mm from sensor on 0.5 mm thick adhesively bonded specimen with configurations: **a** 0.5-0.5-1.5, **b** 0.5-0.5-1.5-25%, **c** 0.5-0.5-1.5-40%, **d** S-1.5-0.5-0.5, **e** S-1.5-0.5-0.5-P-25%, and **f** S-1.5-0.5-0.5-P-40%

shift from the high frequency band to the low frequency band is similar to the behaviour seen with decreasing thickness and the energy distribution within these frequency bands. The cause for this behaviour is expected to be the same as before, increasing defect area along the interface between the adhesive layer and the adherend leads to lower damping of the propagating modes within the metal plate. Since the low

frequency A0 has a higher surface displacement compared to the high frequency A0, upon introduction of the defects, this component seems to reappear. From the analysis, it was seen that the sensitivity of the technique is highest with the configurations where the PLB was carried out on the 0.5 mm plate. This was particularly the case with the 0.1 mm thick adhesive layer bond. As the thickness increased, only configuration

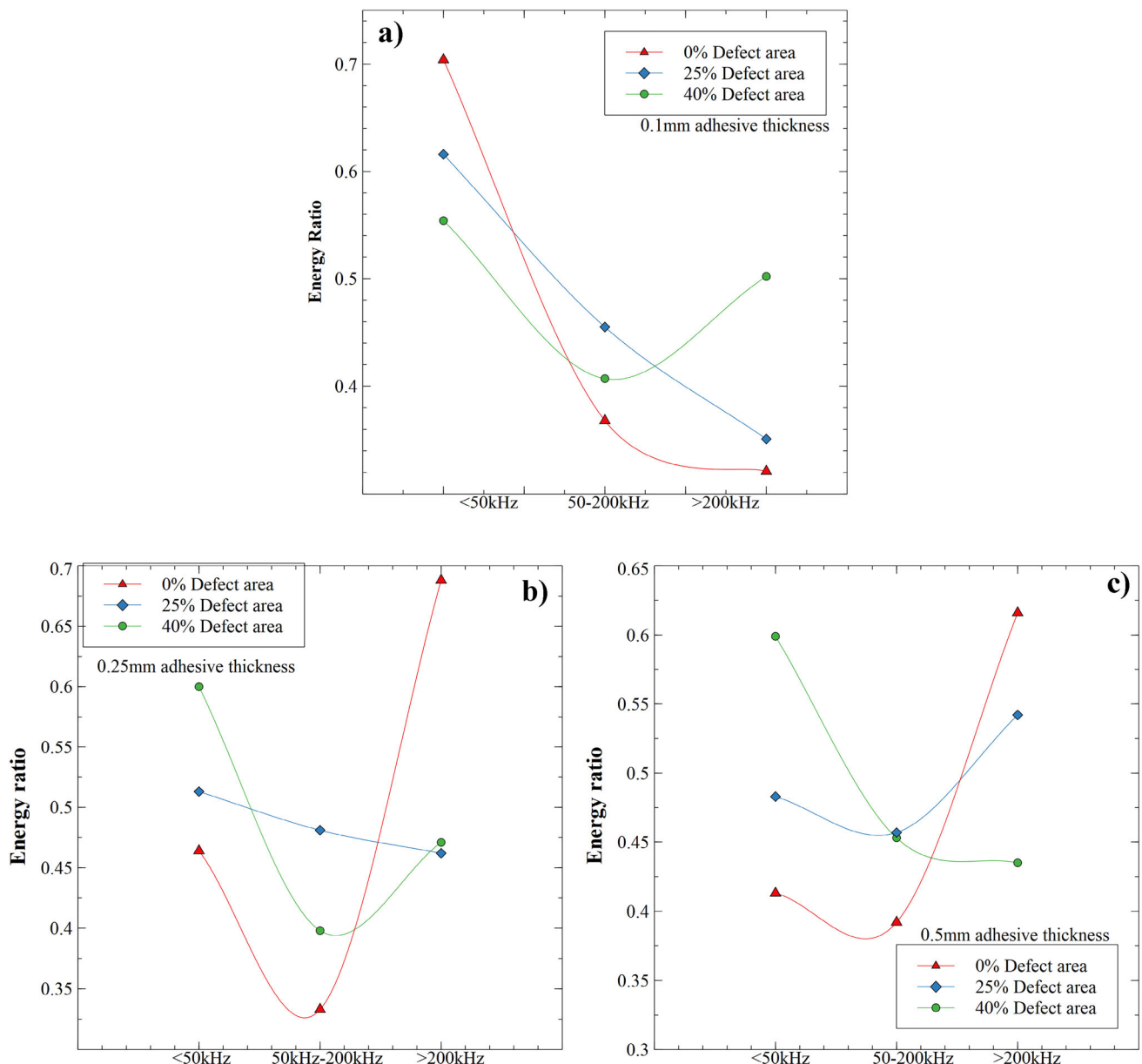


**Fig. 16** Variation of energy ratios of 50 kHz-lowpass, 50–200 kHz bandpass and 200 kHz-Highpass components for various defect areas with a 0.1 mm thick, b. 0.25 mm thick and c 0.5 mm thick adhesive layered bonds in the configuration 0.5-A-1.5

0.5-A-1.5 was seen to be sensitive to the presence of defects. It has to be kept in mind that the interfacial defects are towards the 0.5 mm plate. It is possible that the increased degree of damping made the configuration S-1.5-A-0.5-P sensitive to the difference in the propagating waves. In both the cases, the 200 kHz-highpass component was seen to show high sensitivity to the defects, as seen in Fig. 15. Based on the signal behaviour, the ring down time of the 200 kHz component was calculated for the signals recorded for each specimen type with the configuration 0.5-A-1.5. The duration above threshold of this component was estimated for each specimen type and is shown in Fig. 17 for the 0.1 mm and 0.5 mm

thick adhesive layer bonds. As seen, the obtained values are distinguishable and given the number of PLB repetitions carried out on each specimen, the reliability of this technique is relatively high. It is to be noted that the proposed technique is only capable of detecting the presence of defects and predicting the area of defects but not the location. In this case, the defects were distributed uniformly along the interface.

The present technique considers the energy associated with all the reflections from the specimen edges. In large enough specimens, the edge reflections may not be observed or might be of a very low amplitude owing to the damping induced by the adhesive. From Fig. 13b and c, the WT

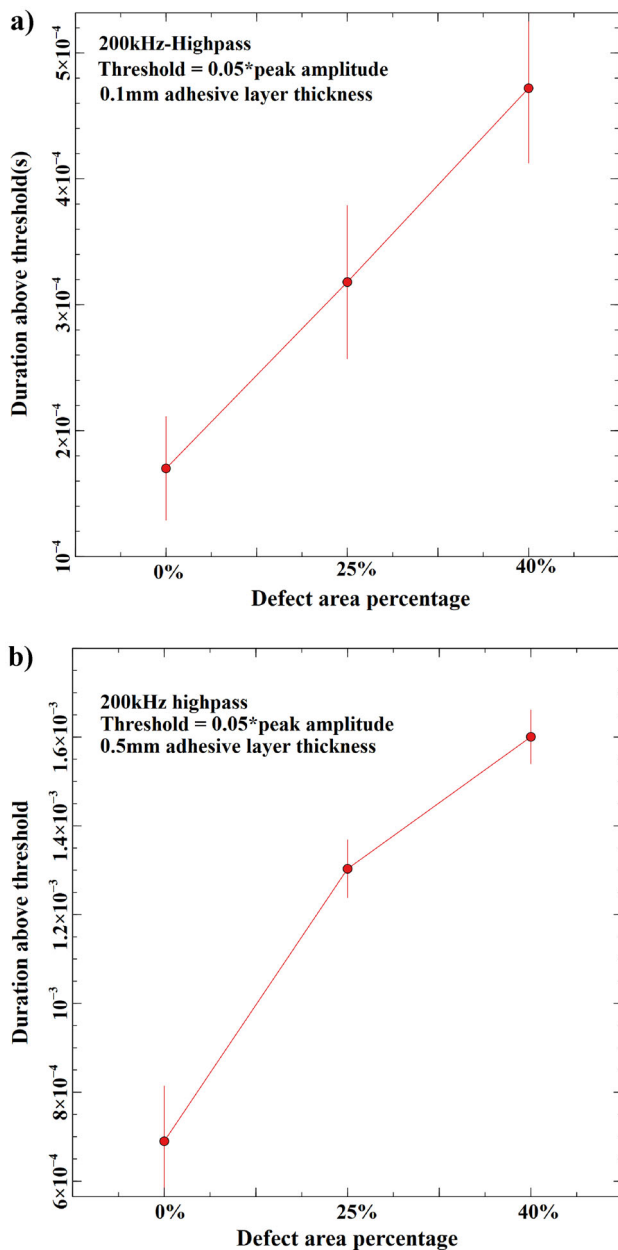


**Fig. 17** a Duration above threshold of the 200 kHz-Highpass component of specimens with a 0.1 mm thick adhesive layer, b 0.5 mm thick adhesive layer in the configuration 0.5-A-1.5

coefficients are higher with the defective specimen. Though it might seem counter-intuitive, it can be inferred that the addition of the PTFE spray along the interface leads to an introduction of a barrier across which the propagating waves are reflected into the metallic plate. This can be further explained by considering the top adherend and the adhesive layer together as a composite plate. Where there is a defect along the interface along the lower adherend, this composite plate acts as if it is freely suspended and fixed along the defect boundary. Upon propagation of plate waves, this plate tends

to vibrate freely. This could be the reason why the configuration with the PLB source and the sensor on the opposite faces was not able to detect the defects. The added attenuation because of the through thickness transmission of the signal added to this. This explanation is supported by the results reported by [19]. They observed that the amplitude of vibration measured using optical fibre interferometry directly on top of an interfacial defect is higher compared to that measured on a fully bonded specimen and this increased with the energy input.

In the presence of a defect, additional mode conversion in adhesive bond was reported [20], where the two bonded surfaces act as independent plates across the interface, with A0 and S0 modes propagating within them separately. Overall, the amplitude of the propagating wave increased with an increase in the defect size. This agrees with the behaviour seen in the current study where the amplitude with the defective joints is higher compared to those of the pristine specimens. In addition, the wave decay with respect to time was also seen to be slower in the defective joints possibly due to the presence of mode conversion. In the presence of a circular defect, trapping of a proportion of the Lamb wave energy in the defective area was reported [10]. In the presence of several such small defects distributed along the interface, significant proportion of the energy can be expected to be trapped in the upper adherend in the current case, which explains the increased activity in the recorded signal with higher defect percentages, as reflected by the durations above threshold. The fundamental asymmetric mode A0 was found to be reflected into the host structure upon incidence on a defect in an adhesively bonded structure. These reflections are minimal in the case of a perfect, flawless bond. This phenomenon was observed through the 200 kHz–600 kHz frequency range and so was proposed as a potential means of detecting kissing bonds. Specifically, simulations showed that a frequency of 400 kHz provides a large enough contrast in a defective bond against a pristine bond. In addition, the mode conversion of S0 to A0 across a defective interface is reported leading to an additional component of wave propagation. However, in the current case, the amplitude of the S0 component induced by the PLB was too small to have multiple reflections.

## 4 Conclusions

In this paper, the feasibility of using PLBs as point sources to detect the presence of interfacial disbond type defects in adhesive bonds has been evaluated. Adhesive layers of three different thicknesses (0.1 mm, 0.25 mm, 0.5 mm) and three different defect areas values (0%, 25%, 40%) have been considered. Four different sensor-source location configurations

have been tested. Based on the findings the following conclusions have been drawn:

- a. The PLB source induces both A0 and S0 wave mode propagation in the adhesive bonds and the individual metal plates. The magnitude of the S0 mode is small and quickly dampens. The A0 mode exhibits dispersion and is predominant in both the adhesive bonded specimens and the metal plates.
- b. The A0 mode is sensitive to the presence of the defects, specifically the A0 mode with a frequency > 200 kHz. The duration above threshold of this component shows a significant difference between the different defect area percentages.
- c. With all the thicknesses, the configurations where the PLB is on the plate closer to the defective interface, i.e., 0.5-A-1.5 was shown to exhibit a noticeable difference in the signal characteristics. The signal travel path through the adhesive layer, seen in the other configurations, induces high enough damping that no significant difference is seen between the different defective specimens at higher thicknesses (0.25 mm, 0.5 mm)
- d. Increase in the thickness of the adhesive layer leads to a change in the energy distribution of the signal in the frequency spectrum due to the relaxation of the constraint exerted by the adherends on the adhesive layer and consequent increase in the damping of lower frequencies.
- e. In the higher thickness adhesive layers, increase in the defect area percentage along the interface reduces the damping of the lower frequencies and a shift in the energy distribution is seen from higher to lower frequencies. This is similar to the effect of adhesive layer thickness reduction.

The proposed method might also be applicable to larger specimen sizes given the low decay rates of guided Lamb waves in thin metal plates. Large specimen areas can be quickly evaluated for defects using the proposed method owing to its ease of use. However, the effect of larger specimen dimensions on the presence of edge reflections in the signal records has to be evaluated. In the current analysis, edge reflections have been considered. Further work is required to establish the defect location and sizing based on the PLB induced wave propagation in adhesive bonds in both the specimens used in this study and larger specimens.

**Acknowledgements** This research was carried by the lead author as part of fully funded PhD studentship provided by the School of Engineering, Robert Gordon University, UK.

**Data Availability** The data that supports the findings of this study is available from the corresponding author upon reasonable request.

## Declarations

**Conflict of interest** The authors report no conflict of interests.

**Open Access** This article is licensed under a Creative Commons Attribution 4.0 International License, which permits use, sharing, adaptation, distribution and reproduction in any medium or format, as long as you give appropriate credit to the original author(s) and the source, provide a link to the Creative Commons licence, and indicate if changes were made. The images or other third party material in this article are included in the article's Creative Commons licence, unless indicated otherwise in a credit line to the material. If material is not included in the article's Creative Commons licence and your intended use is not permitted by statutory regulation or exceeds the permitted use, you will need to obtain permission directly from the copyright holder. To view a copy of this licence, visit <http://creativecommons.org/licenses/by/4.0/>.

## References

1. Kumar, R.L.V., Bhat, M.R., Murthy, C.R.L.: Some studies on evaluation of degradation in composite adhesive joints using ultrasonic techniques. *Ultrasonics* **53**(6), 1150–1162 (2013). <https://doi.org/10.1016/j.ultras.2013.01.014>
2. Rucka, M., Wojtczak, E., Lachowicz, J.: Detection of debonding in adhesive joints using Lamb wave propagation. *MATEC Web Conf.* **262**, 10012 (2019). <https://doi.org/10.1051/mateconf/201926210012>
3. Najib, M.F., Nobari, A.S.: Kissing bond detection in structural adhesive joints using nonlinear dynamic characteristics. *Int. J. Adhes. Adhes.* **63**, 46–56 (2015). <https://doi.org/10.1016/j.ijadhadh.2015.08.004>
4. Droubi, M.G., Faisal, N.H., Orr, F., Steel, J.A., El-Shaib, M.: Acoustic emission method for defect detection and identification in carbon steel welded joints. *J. Constr. Steel Res.* **134**, 28–37 (2017). <https://doi.org/10.1016/j.jcsr.2017.03.012>
5. Sause, M.: Investigation of pencil-lead breaks as acoustic emission sources. *J. Acoust. Emiss.* **29**, 184–196 (2011)
6. Hamstad, M.A.: Acoustic emission signals generated by monopole (pencil-lead break) versus dipole sources: finite element modeling and experiments. *J. Acoustic Emission* **25**, 92–106 (2007)
7. Zelenyak, A.M., Hamstad, M.A., Sause, M.G.R.: Modeling of acoustic emission signal propagation in waveguides. *Sensors (Switzerland)* **15**(5), 11805–11822 (2015). <https://doi.org/10.3390/s150511805>
8. Rokhlin, S.I.: Lamb wave interaction with lap-shear adhesive joints: theory and experiment. *J. Acoust. Soc. Am.* **89**(6), 2758–2765 (1991). <https://doi.org/10.1121/1.400715>
9. Marks, R., Clarke, A., Featherston, C., Paget, C., Pullin, R.: Lamb wave interaction with adhesively bonded stiffeners and disbonds using 3D vibrometry. *Appl. Sci.* (2016). <https://doi.org/10.3390/app6010012>
10. Ong, W.H., Rajic, N., Chiu, W.K., Rosalie, C.: Lamb wave-based detection of a controlled disbond in a lap joint. *Struct. Heal. Monit.* **17**(3), 668–683 (2018). <https://doi.org/10.1177/1475921717715302>
11. K. Diamanti, J. M. Hodgkinson, and C. Soutis, Application of a lamb wave technique for the non-destructive inspection of composite structures. pp. 1–10.
12. Mustapha, S., Ye, L., Dong, X., Alamdari, M.M.: Evaluation of barely visible indentation damage (BVID) in CF/EP sandwich composites using guided wave signals. *Mech. Syst. Signal*

- Process. **76–77**, 497–517 (2016). <https://doi.org/10.1016/j.ymsp.2016.01.023>
13. Rucka, M., Wojtczak, E., Lachowicz, J.: Damage imaging in lamb wave-based inspection of adhesive joints. *Appl. Sci.* (2018). <https://doi.org/10.3390/app8040522>
  14. Mori, N., Wakabayashi, D., Hayashi, T.: Tangential bond stiffness evaluation of adhesive lap joints by spectral interference of the low-frequency A0 lamb wave. *Int. J. Adhes. Adhes.* **113**, 103071 (2022). <https://doi.org/10.1016/j.ijadhadh.2021.103071>
  15. A.K. Prathuru, Structural and residual strength analysis of metal-to-metal adhesively bonded joints. Robert Gordon University [online], PhD thesis, 2019. Available from: <https://rgu-repository.worktribe.com/output/346900>
  16. ASTM: E 976–99, Standard Guide for Determining the Reproducibility of Acoustic Emission Response, pp. 1–7, 2009.
  17. Sause, M.G.R., Horn, S.: Simulation of acoustic emission in planar carbon fiber reinforced plastic specimens. *J. Nondestruct. Eval.* **29**(2), 123–142 (2010). <https://doi.org/10.1007/s10921-010-0071-7>
  18. Crawford, A., Droubi, M.G., Faisal, N.H.: Analysis of acoustic emission propagation in metal-to-metal adhesively bonded joints. *J. Nondestruct. Eval.* **37**(2), 1–19 (2018). <https://doi.org/10.1007/s10921-018-0488-y>
  19. Heller, K., Jacobs, L.J., Qu, J.: Characterization of adhesive bond properties using Lamb waves. *NDT E Int.* **33**(8), 555–563 (2000). [https://doi.org/10.1016/S0963-8695\(00\)00022-0](https://doi.org/10.1016/S0963-8695(00)00022-0)
  20. Mai, A.K., Xu, P.C., Bar-Cohen, Y.: Leaky lamb waves for the ultrasonic nondestructive evaluation of adhesive bonds. *J. Eng. Mater. Technol. Trans. ASME* **112**(3), 255–259 (1990). <https://doi.org/10.1115/1.2903319>

**Publisher's Note** Springer Nature remains neutral with regard to jurisdictional claims in published maps and institutional affiliations.